



## Performance Enhancement of M-ary DPPM Bit Error Rate in FSO Systems with Aperture Averaging Under Crosstalk, Pointing Error, and ASE Noise Conditions

Ebrahim Eldesoky Elsayed\*<sup>1</sup>, Mohammed Raisan Hayal<sup>2</sup>

<sup>1</sup>Department of Electronics and Communications Engineering, Faculty of Engineering, Mansoura University, Mansoura, Egypt; e-mail addresses: engebrahim16@gmail.com; engebrahim16@std.mans.edu.eg; ORCID ID: <https://orcid.org/0000-0002-7208-2194>

<sup>2</sup>Department of Electronics and Communications Engineering, Faculty of Engineering, Mansoura University, Mansoura, Egypt; (e-mail: mohammedraisan@gmail.com); ORCID ID: <https://orcid.org/0000-0002-7997-702X>

\*Corresponding Author E-Mail ID address: Ebrahim Eldesoky Elsayed (engebrahim16@gmail.com)

Cite this study: Elsayed, E. E., Hayal, M. R. (2024). Performance Enhancement of M-ary DPPM Bit Error Rate in FSO Systems with Aperture Averaging Under Crosstalk, Pointing Error, and ASE Noise Conditions. *Engineering Applications*, 3 (2), 125-136.

### Keywords

amplified spontaneous emission, pointing error, digital pulse position modulation, free-space optical (FSO) communication, modified Chernoff bound, aperture-averaging.

### Research Article

Received:09.03.2024

Revised:15.03.2024

Accepted:29.07.2024

Published:30.08.2024

### Abstract

The evaluation of the performance of a communication system based on free-space optical (FSO) technology using digital pulse position modulation (DPPM) and on-off keying non-return-to-zero (OOK-NRZ) technique is explored within this study. This research delves into the effects of atmospheric turbulence, scintillation, and amplified spontaneous emission (ASE) noise. In order to mitigate the impact of turbulence-induced scintillation and optical power loss, the utilization of aperture averaging is suggested. The assessment of bit-error rate (BER) performance under atmospheric turbulence and ASE noise is detailed, employing moment generation function techniques in conjunction with a modified Chernoff bound for enhanced accuracy compared to the conventional Chernoff bound. This system shows potential for providing power-efficient, cost-effective, highly flexible, and reliable solutions for future access networks catered towards higher data rates. BER results are presented for an optically preamplified DPPM FSO communication system affected by pointing errors, atmospheric turbulence, and ASE noise from optical amplification. The use of a gamma-gamma distribution model enables the characterization of various turbulence conditions. The findings showcase the superiority of DPPM in terms of enhanced receiver sensitivity, with an improvement of approximately 10 dB – 11 dB over an equivalent optically preamplified OOK-NRZ approach at a binary data rate of 2.5 Gbps and a typical FSO BER of  $10^{-9}$ ), contingent on the turbulence levels.



## 1. Introduction

In recent years, there has been a resurgence of interest in exploring and harnessing free-space optical (FSO) communication. This interest has been sparked by the substantial potential bandwidth available in comparison to

radio frequency (RF) and the enhanced flexibility when compared to traditional optical fiber networks. FSO communication typically involves sending information-carrying near-infrared light through the atmosphere between multiple transceivers. It has now been established as a commercially viable counterpart to RF and millimeter-wave systems [1–3]. In the realm of FSO communication, an optical preamplifier setup is commonly utilized to boost power at the photodetector, ultimately enhancing receiver sensitivity. However, this advantageous setup also presents challenges, particularly in managing the signal-to-noise ratio (SNR) degradation due to amplified spontaneous emission (ASE) noise resulting from optical amplification. This noise gives rise to signal spontaneous and spontaneous-spontaneous beat noises, in addition to the typical electrical domain noise. Wavelength-division multiplexing (WDM) systems find application in both optical fiber and FSO networks [4], [5–7]. In the context of WDM-PON (Passive Optical Network), specific wavelengths are designated for each Optical Network Unit (ONU), thereby fully leveraging the abundant transmission bandwidth available in the optical domain and circumventing the synchronization and threshold requirements associated with burst mode upstream of time-division multiplexing/time division multiple access (TDM/TDMA) systems [7, 8]. As the need for bandwidth continues to rise, WDM systems have been explored and increasingly implemented in fiber, free-space, and wireless optical networks [7, 9–11]. Dense wavelength division multiplexing (DWDM) technology can cater to multi-user access scenarios, with DWDM-PON emerging as a promising solution to the escalating bandwidth demands of future access networks. It offers the potential for higher data rates, improved data security, and extended reach [7, 9, 12]. Compared to TDM/TDMA PONs, WDM PON systems provide additional benefits such as reduced loss, enhanced security (owing to dedicated wavelengths), longer reach, and are being seen as a primary solution to the growing bandwidth requirements in access networks [7, 13, 14]. In contrast to space-division multiplexing, DWDM facilitates network resource sharing, thereby lowering implementation costs. Unlike code-division multiplexing or traditional TDM systems where the system bit rate and chip rate might exceed the end user's data rate, DWDM systems enable all users to simultaneously transmit at the full system bit rate. The bit rate and chip rate in DWDM systems may exceed the end user's data rate, enabling simultaneous transmission by all users at a full system bit rate limited only by electronic processing speed [4, 7]. Digital pulse-position modulation (DPPM) has found success in fiber, intersatellite, and deep space optical communication systems, positioning itself as a promising choice for terrestrial FSO systems [7, 15, 16]. Despite the advantages of the DPPM format, it does require greater channel bandwidth. Studies on FSO systems have demonstrated that digital pulse modulation schemes are more power-efficient compared to on-off keying (OOK) and are particularly suitable for FSO communication systems where dispersion is minimal [7, 17, 18, 19]. FSO systems face challenges from pointing errors (PE) caused by inaccurate tracking systems or mechanical vibrations induced by natural elements like strong winds, thermal expansion, or minor earthquakes [7, 20, 21]. These PE factors can limit the optimal performance of the FSO system. To address performance degradation due to PE, turbulence, coupling, and atmospheric losses, optical amplification is included [7, 17, 22]. This study focuses on the combined impacts of atmospherically induced scintillation and PE on an optically preamplified FSO system, integrating PE analyses from [3, 4] with the Bit Error Rate (BER) evaluations conducted by the present authors in previous work [7, 17, 22]. Yamamoto [23] developed expressions for the mean and variance of an optically preamplified signal to facilitate a Gaussian approximation (GA). However, this GA approach does not fully encompass the signal plus ASE noise distribution, which is not strictly Gaussian but rather related to chi-square (ASE only) and non-central chi-square (signal plus ASE) distributions [7]. Various diversity techniques have been proposed in literature to counter turbulence-induced scintillation in FSO communication systems, including time diversity, spatial diversity with multiple transmitters/receivers, and aperture averaging (AA) [1, 3, 7]. Given the simplicity and effectiveness of aperture averaging, its impact on different regimes (WT, MT, and ST) will be examined in this study. Personick [24] and later Ribeiro et al. [25] introduced alternative formulations based on a moment generating function (MGF) that provides a comprehensive statistical description of a system utilizing an optically preamplified direct detection receiver. The Bit Error Rate (BER) for OOK systems in [23–25] is then assessed using MGF-based techniques like Chernoff bound (CB) and modified Chernoff bound (MCB). Various distributions such as lognormal (LN), gamma-gamma (GG), K (KD), and negative exponential (NE) are used in this study, with results compared against the conventional GA approach. This paper is structured as follows: Section 2 elaborates on the optically preamplified receiver. Section 3 presents the DPPM crosstalk. Section 4 evaluates of the atmospheric turbulence models. Section 5 evaluates the moment generation function analysis. Section 6 introduces the bit-error rate (BER) analysis. Section 7 shows the results and discussions. Section 8 concludes this paper.

## **2. Optically Preamplified Receiver**

Enhancing the performance of a conventional positive-intrinsic-negative (PIN) direct detection receiver setup for an FSO communication system is achievable by integrating an optical preamplifier following the receiver collecting lens (RCL), as illustrated in Figure 1. An optical amplifier with gain  $G$  and noise figure  $NF$  is positioned before the photodiode, where the incoming optical signal is introduced via a collimator into a short fiber that feeds into the optical amplifier. Between the optical amplifier and the photodiode, an optical bandpass filter (OBPF) with

an optical bandwidth  $B_o$  is situated [7]. Within this receiver configuration, the receiver collecting lens (RCL) is assumed to be perfectly aligned with the transmitter lens in a pointing and tracking scheme. It captures the incident laser beam, which is then fed into a fiber using a collimator before undergoing optical amplification [7, 26]. The optical pre-amplification process introduces Amplified Spontaneous Emission (ASE) noise, statistically characterized as Gaussian field. The optical amplifier  $G$  provides gain. Besides the amplified optical signal, ASE noise is generated, with a power spectral density  $N_o = 0.5(NF \times G - 1) E$  (in a single polarization), where  $E$  represents photon energy and  $NF$  is the noise figure. In the electrical domain, the ASE noise interacts with the signal and itself, resulting in the formation of signal-spontaneous and spontaneous-spontaneous beat noises [7]. The optical bandpass filter, with a bandwidth  $B_o$ , comes before the pin photodiode (with a quantum efficiency  $\eta$ ), helping to diminish the incident ASE power on the photodiode. The decision circuitry is characterized by an integrate-and-dump filter across  $t_s$ . The outcomes obtained per frame are compared to determine the slot (and consequently the word) with the highest value.  $M_t$  represents the number of polarization modes for ASE noise, and  $R = \eta / E$  [7].

### 3. DPPM Crosstalk

Digital pulse position modulation (DPPM) is one of the schemes that use the time-varying properties of a pulse train, with each data binary-word submitted by the distinct position of a signal pulse in a time frame [7]. In the DPPM scheme illustrated in Fig. 2, a frame of duration equal to  $MT_b$  is divided into  $n=2^M$  equal time slots of length  $t_s = MT_b/n$ , where  $M$  is the coding level and is equal to the number of data bits transmitted per DPPM frame. Also,  $T_b = 1/R_b$  is the equivalent OOK-NRZ bit period and  $R_b$  is the raw bit rate [7]. An input word is then represented by placing an optical pulse in one of the DPPM time slots in the frame. In this analysis, the incident DPPM signal is detected by integrating over each DPPM slot and comparing the outcomes across the frame to identify the highest result [7, 15, 27]. This method brings about an increase in bandwidth efficiency, particularly favored at higher coding levels or bit resolutions. Additionally, DPPM necessitates a precise synchronization unit, adding to receiver complexity. In scenarios involving dispersive channels like optical fibers, guard bands are vital to distinguish one signal frame from another. Each frame comprises a single pulse occupying a DPPM slot, and the position of the pulse within the frame corresponds to the value of the  $M$ -bit word. In Fig. 2, the OOK-NRZ and its equivalent 16-DPPM signal are depicted. The attainment of timing synchronization has been a subject of investigation in FSO systems [7, 28, 29]. Moreover, the DPPM receiver is managed by slot synchronization and frame synchronization circuits, as illustrated in Figure 1.

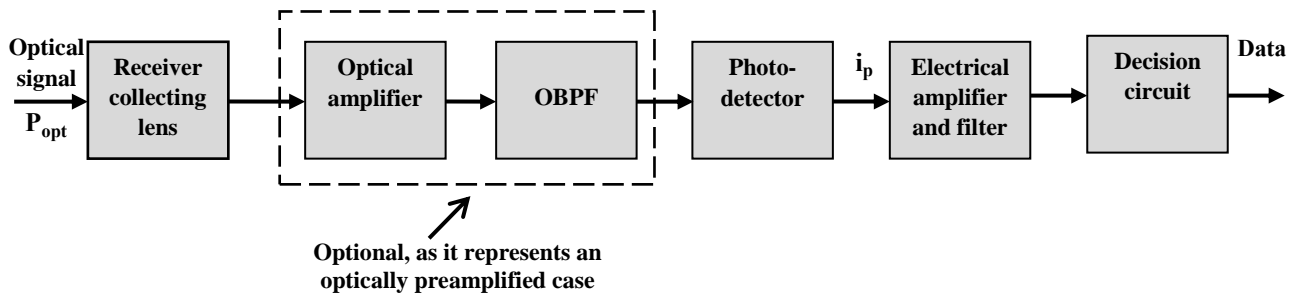


Figure 1. Block diagram of optically FSO receiver

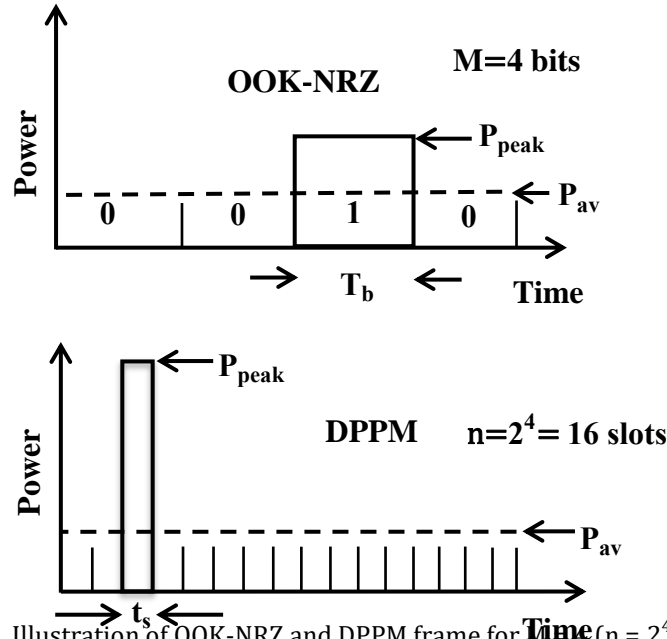


Figure 2. Illustration of OOK-NRZ and DPPM frame for  $M=4$  bits ( $n = 2^4 = 16$  slots)

#### 4. Atmospheric Turbulence Models

In conditions of clear air, the propagation of optical beams through the atmosphere is notably impacted by turbulence-induced scintillation, leading to a substantial decrease in link performance [1, 7, 30, 31]. The primary effect of scintillation is the variability in irradiance levels at the receiver, leading to elevated Bit Error Rates (BERs) [1]. Equation (1) demonstrates the relationship between Rytov variance and refractive index structure. The Gamma-Gamma distribution is calculated from Eq. (2). FSO links are commonly classified into various levels of turbulence using the Rytov variance  $\sigma_R^2$ , which is given by [1, 3, 7, 30, 32, 33]

$$\sigma_R^2 = 1.23 C_n^2 k^{7/6} l_{fso}^{11/6} \quad (1)$$

where  $C_n^2$  is the refractive index structure constant takes values typically within (ranging from  $\approx 10^{-17} \text{m}^{-2/3}$  to  $\approx 10^{-13} \text{m}^{-2/3}$ ) [3, 7, 30],  $l_{fso}$  is the FSO link length,  $k = 2\pi/\lambda$  is the wave number, and  $\lambda$  is the wavelength [7, 29, 30, 33]. The Rytov variance distinguishes the various link turbulence regimes  $\sigma_R^2$  if the resulting  $\sigma_R^2 < 1$ , we have weak turbulence (WT); if  $\sigma_R^2 \approx 1$ , we have moderate turbulence (MT) and if  $\sigma_R^2 > 1$ ; we have strong turbulence (ST), and if saturated turbulence  $\sigma_R^2 \rightarrow \infty$  are given as from [1, 3, 7, 30]. The effects of turbulence are characterized using the gamma-gamma (GG) probability density function (pdf), which is given as [1, 3, 7, 30, 32, 33]

$$p_{GG}(h_{\text{turb}}) = \frac{2(\alpha\beta)^{(\alpha+\beta)/2}}{\Gamma(\alpha)\Gamma(\beta)} h_z^{((\alpha+\beta)/2)-1} K_{\alpha-\beta}(2\sqrt{\alpha\beta h_{\text{turb}}}); \quad h_{\text{turb}} > 0 \quad (2)$$

where  $h_{\text{turb}}$  is the attenuation because of atmospheric turbulence,  $\alpha$  and  $\beta$  are the effective number of large-scale and small-scale eddies of the scattering process, respectively,  $K_n(\cdot)$  is the modified Bessel function of second kind, order  $n$  and  $\Gamma(\cdot)$  is the gamma function. The signal and interferer travel over physically distinct paths in the upstream and thus have uncorrelated turbulence; hence, their GG pdfs are each treated independently. The parameter  $\alpha$  and  $\beta$  for plane-wave propagation for arbitrary aperture size are calculated from Eqs. (3) and (4) respectively [1, 3, 7, 33]

$$\alpha = \left\{ \exp \left[ \frac{0.49\sigma_R^2}{\left(1 + 0.65d^2 + 1.11\sigma_R^{12/5}\right)^{7/6}} \right] - 1 \right\}^{-1}, \quad (3)$$

$$\beta = \left\{ \exp \left[ \frac{0.51\sigma_R^2 \left(1 + 0.69\sigma_R^{12/5}\right)^{-5/6}}{1 + 0.9d^2 + 0.62d^2\sigma_R^{12/5}} \right] - 1 \right\}^{-1}, \quad (4)$$

$$d = \sqrt{kD_{RX}^2 / 4l_{fso}} \quad (5)$$

where  $d$  is the normalized receiver collecting lenses normalized (RCLs) as shown in Eq. (5) [7, 30, 33], Aperture averaging (AA) is a commonly used method for mitigating turbulence-induced scintillation [1, 3, 7, 33, 34, 35]. This method essentially entails increasing the RCL area such that it is larger than the fluctuating irradiance correlation width  $\rho_o = (1.46C_n^2 k^2 l_{fso})^{-3/5}$  [1], resulting in averaging of the irradiance fluctuations over the RCL area such that a significant reduction in scintillation is achieved compared to that observed for a point receiver [1, 3, 33–35]. The decrease in irradiance fluctuation is typically measured using the AA factor  $A = \sigma_I^2(D_{RX})/\sigma_I^2(0)$  [33], where  $\sigma_I^2(D_{RX})$  is the scintillation index for RCL diameter  $D_{RX}$  ( $D_{RX} = 0$  for a point receiver) and is given as [7, 33]

### 5. Moment Generation Function Analysis

For a given irradiance  $I$  the optical power at the optical amplifier input during OOK NRZ bit of data  $j \in \{0, 1\}$  is expressed mathematically in Eq. 6 [7]

$$P_j(I) = a_j I A \quad (6)$$

where  $a_1 = 2r/(r + 1)$ ,  $a_0 = 2/(r + 1)$ ,  $A$  is the area of the receiver aperture and  $r$  is the extinction ratio (typically 10). Clearly,  $I$  is the mean irradiance for the bit stream at a particular time. The MGF (conditional on  $I$ ) can then be obtained from, for example [7, 25], under the assumption of an integrating response over bit period  $T$  (which has a noise equivalent bandwidth  $B_e = 1/2T$ ) [7, 22]

$$M_{Y_j}(s/I) = \frac{\exp \left[ R' G s q P_j(I) / \left( 1 - (R' N_0 s q / T) \right) \right]}{\left[ 1 - (R' N_0 s q / T) \right]^L} \quad (7)$$

where  $q$  is the electron charge,  $s$  is the standard parameter in the transform domain for the MGF in Eq. (7),  $L = B_0 m_t T$  is the product of spatial and temporal modes,  $B_0$  is the OBPB bandwidth in Hz,  $m_t = 2$  is number of polarization modes,  $N_0 = n_{sp}(G - 1)hf$  is the ASE power spectral density (PSD) in W/Hz (in single polarization),  $n_{sp}$  is the spontaneous emission factor,  $R' = \eta/hf$ ,  $G$  is the optical amplifier gain,  $h$  is the Planck's constant and  $f$  is the optical frequency in Hz. On introducing the Gaussian receiver thermal noise, a new overall conditional MGF for the signal at the decision device is obtained from Eq. (8) [25]

$$\begin{aligned} M_{Z_j}(s/I) \\ = M_{th}(s) M_{Y_j}(s/I) \end{aligned} \quad (8)$$

where  $M_{th}(s) M_{Y_j} = \exp(\sigma_{th}^2 s^2 / 2)$  is the thermal noise MGF and  $\sigma_{th}^2$  is the thermal noise variance at the decision circuit. The conditioning of the MGF on  $I$  will be removed in the BER calculation in the next section.

### 6. Bit-Error Rate Analysis

In this section, the application of MGF methods, specifically the CB and MCB for the BER evaluation is presented for weak-to-strong turbulence regimes, using the LN, GG, KD and NE atmospheric turbulence models. The BER for a given irradiance  $I$  is given in Eq. (9) [7, 17]

$$\begin{aligned} \text{BER}(I) = \frac{1}{2} [ & P(1|0, I) \\ & + P(0|1, I) ] \end{aligned} \quad (9)$$

where  $P(1|0, I)$  represents the probability of receiving a 1 given that 0 was transmitted and  $P(0|1, I)$  represents the probability of receiving a 0 given that 1 was transmitted. On applying the CB separately to each conditional probability, (9) and (10) are obtained [7, 17]

$$P(1|0, I) = P(i_0(I) > i_D(I)) \leq \exp(-s_0 i_D(I)) M_{Z_0}(s_0, I), \quad s_0 > 0 \quad (10)$$

$$P(0|1, I) = P(i_1(I) > i_D(I)) \leq \exp(-s_1 i_D(I)) M_{Z_1}(-s_1, I), \quad s_0 > 0 \quad (11)$$

where  $i_D(I)$  is the decision threshold as shown in Eqs. (10) and (11). The CB therefore gives the upper bound on the BER as [7]

$$\text{BER}_{\text{CB}}(I) = \frac{1}{2} \left[ \exp(-s_0 i_D(I)) M_{Z_0}(s_0, I) + \exp(s_1 i_D(I)) M_{Z_1}(-s_1, I) \right]_{s=s_0=s_1 > 0} \quad (12)$$

where  $M_{Z_0}(s, I)$  and  $M_{Z_1}(s, I)$  are given by Eqs. (8) and (12). The setting of  $s = s_0 = s_1$  is a computational convenience that incurs a very small accuracy penalty (as  $s_0$  and  $s_1$  can of course be optimized separately) [25]. By replacing the optical link length  $z$  with  $l_{\text{fso}}$ . The beam width of a Gaussian laser beam  $w_z$  due to diffraction and turbulence effects grows with the optical link length  $z = l_{\text{fso}}$ , and it is calculated from Eq. (13) [1, 7]

$$w_z = w_0 \left( \sqrt{1 + (z/z_L)^2} \right) \left( \sqrt{1 + 1.33 \sigma_R^2 \left( 2z/kw_0 \sqrt{1 + (z/z_L)^2} \right)^{5/6}} \right) \quad (13)$$

where  $w_0$  is the minimum value of  $w_z$  at a point ( $z = 0$ ) along the beam axis and  $z_L = \pi w_0^2 / 2$  is called the Rayleigh range. The Gaussian beam at the receiver is approximated as plane wave for aspects such as the turbulence modelling and the beam characterization of this analysis, though the pointing error analysis relies on its Gaussian nature. The pdf for attenuation due to PE and geometric spread (GS) is given in Eq. (14) [7, 20, 21]

$$p_{PE}(h_p) = \frac{\gamma^2}{A_0^{\gamma^2}} h_p^{\gamma^2-1}; \quad 0 \leq h_p \leq A_0, \quad (14)$$

where  $h_p$  is attenuation due to GS and PE,  $\gamma = w_{z_{\text{eq}}} / 2\sigma_{PE}$ , jitter-induced PE standard deviation at the receiver is  $\sigma_{PE}$ ,  $w_{z_{\text{eq}}}^2 = w_z^2 \sqrt{\pi} \text{erf}(\nu) / 2\nu \exp(-\nu^2)$  is the (square of the) equivalent beam width [7],  $A_0 = [\text{erf}(\nu)]^2$  is the fraction of the collected power at receiver radial displacement of zero [7], and  $\nu = (\sqrt{\pi} r_{\text{RX}}) / (\sqrt{2} w_z)$ . The combined pdf for attenuation due to turbulence, PE and GS can then be expressed as [7, 20, 21]

$$p(h_{\text{tot}}) = \int p_{PE}(h_{\text{tot}}|h_a) p_{\text{GG}}(h_a) dh_a, \quad (15)$$

where  $h_{\text{tot}} = h_a h_p$  and  $p_{PE}$  is the probability distribution for PE conditioned on  $h_a$  as shown in Eq. (15) and (16), such that [7, 36]

$$\int p_{PE}(h_{\text{tot}}|h_a) = \frac{1}{h_a} p_{PE}\left(\frac{h_{\text{tot}}}{h_a}\right) = \frac{\gamma^2}{A_0^{\gamma^2}} \left(\frac{h_{\text{tot}}}{h_a}\right)^{\gamma^2-1}; \quad 0 \leq h_{\text{tot}} \leq A_0. \quad (16)$$

On substituting Eq. (2) and Eq. (16) into Eq. (15), the combined pdf can be re-written in Eq. (17) [7, 36]

$$p_{\text{GG}}(h_{\text{tot}}) = \frac{2\gamma^2(\alpha\beta)^{(\alpha+\beta)/2}}{A_0^{\gamma^2} \Gamma(\alpha) \Gamma(\beta)} h_{\text{tot}}^{\gamma^2-1} \int_{h_{\text{tot}}/A_0}^{\infty} h_a^{\frac{(\alpha+\beta)}{2}-1-\gamma^2} K_{\alpha-\beta}(2\sqrt{\alpha\beta h_a}) dh_a; \quad (17)$$

The DPPM BER is given by [3, 8, 15] in Eq. (18), here noting the dependence on  $h_{\text{turb}}$  relevant to the current discussion

$$\text{BER}(h_{\text{turb}}, P) = \frac{n P_{\text{We}}(h_{\text{turb}}, P)}{2(n-1)} \quad (18)$$

where  $P_{we}(h_{turb}, P)$  is the symbol error probability. Following the treatment of [15], given that each transmitted word has equal probability, the probability of successful reception of a word  $P_{ws}(h_{turb}, P) = 1 - P_{we}(h_{turb}, P)$  is bounded by exploiting the fact that for a particular frame, the events  $\{X_{tr} > X_1\}, \dots, \{X_{tr} > X_j\}, \dots, \{X_{tr} > X_n\}$  (excluding, the case of  $j = tr$ ) are each no less likely to occur given that any combination of the others have also occur and can expressed in Eqs. (19) and (20), respectively [17, 37-42]

$$\begin{aligned}
 &P_{ws}(h_{turb}, P) \\
 &\geq \prod_{\substack{j=1 \\ j \neq tr}}^n P(X_{tr} > X_j | h_{turb}, P) \\
 &= (P(X_{tr} > X_f | h_{turb}, P))^{n-1}
 \end{aligned} \tag{19}$$

Then  $P_{we}(h_{turb}, P)$  can be expressed as [15]

$$\begin{aligned}
 &P_{we}(h_{turb}, P) \\
 &\leq 1 - (P(X_f > X_{tr} | h_{turb}, P))^{n-1}
 \end{aligned} \tag{20}$$

Under the assumption that the random variables  $X_{tr}$  and  $X_f$  are Gaussian, the GA expression in Eq. (21) for  $P_{we, GA}(h_{turb}, P)$  is given by using Eq. (20) [7, 15]

$$\begin{aligned}
 &P_{we, GA}(h_{turb}, P) \leq 1 - \left( 1 - 0.5 \operatorname{erfc} \left( \frac{\mu_{X_{tr}}(h_{turb}, P) - \mu_{X_f}}{\sqrt{2(\sigma_{X_{tr}}^2(h_{turb}, P) + \sigma_{X_f}^2)}} \right) \right)^{n-1} \\
 &\tag{21}
 \end{aligned}$$

The application of an upper bound upon  $P_{we}(h_{turb}, P)$  using CB technique will also yield upper bound upon  $P(X_f > X_{tr})$ ; hence for  $s > 0$ , the CB is computed in Eq. (22)

$$\begin{aligned}
 &P(X_f > X_{tr} | h_{turb}, P) \\
 &\leq M_{X_f}(s | h_{turb}, P) M_{X_{tr}}(-s | h_{turb}, P) \quad (s > 0)
 \end{aligned} \tag{22}$$

The tightest CB can be obtained by finding the optimum value of  $s$  (i.e.  $s_{opt}$ ) in Eq. (23) [15]

$$\begin{aligned}
 &P_{we, CB}(h_{turb}, P) \leq 1 - \left( 1 - M_{X_{tr}}(-s_{opt} | h_{turb}, P) M_{X_f}(s_{opt} | h_{turb}, P) \right)^{n-1} \\
 &\tag{23}
 \end{aligned}$$

The general case for the MCB is  $P(X > \varphi) \leq \exp(-s\varphi) M_X(s) / s\sigma_{th}\sqrt{2\pi}$  where  $\varphi$  is fixed and  $X$  includes a Gaussian component of variance  $\sigma_{th}^2$ . In comparing  $X_f$  and  $X_{tr}$  whose Gaussian components each have variance  $\sigma_{th}^2$ , the effective variance of the Gaussian contribution becomes  $\sigma_{th}^2 = 2\sigma_{th}^2$  so yielding as expressed in Eq. (24) [17]

$$\begin{aligned}
 &P(X_f > X_{tr} | h_{turb}, P) \leq \\
 &\frac{M_{X_f}(s | h_{turb}, P) M_{X_{tr}}(-s | h_{turb}, P)}{s\sigma_{th}\sqrt{2\pi}}
 \end{aligned} \tag{24}$$

This MCB expression Eq. (24) is then used, with Eq. (20), to obtain

$$\begin{aligned}
 &P_{we, MCB}(h_{turb}, P) \leq 1 - \left( 1 - \left( \frac{M_{X_{tr}}(-s_{opt} | h_{turb}, P) M_{X_f}(s_{opt} | h_{turb}, P)}{2s\sigma_{th}\sqrt{2\pi}} \right) \right)^{n-1} \\
 &\tag{25}
 \end{aligned}$$

The overall DPPM BER is calculated in Eq. (26)

$$\text{BER}_{Z,GG}(P) = \int_0^\infty \text{BER}_Z(h_{turb}, P) p_{GG}(h_{turb}) dh_{turb} \quad (26)$$

where  $\text{BER}_Z(h_{turb}, P)$  represents the BERs obtainable from Eq. (18) using the  $P_{we}(h_{turb}, P)$  bounds of Eq. (21), Eq. (23) and Eq. (25) ( $Z = \text{GA, CB and MCB}$ ) while  $p_{GG}(h_{turb})$  represents the GG atmospheric turbulence model given in Eq. (2). Hence, to perform the integration in Eq. (26) numerically, the  $s_{opt}$  must be found for each step in the integration [37-42].

### 7. Results and Discussions

The parameters used in this model are presented in Table 1 for [17], [42], and [Present Work Proposed]. Table 2 shows the design parameters required for a FSO link. Three different atmospheric conditions characterized by the refractive-index structure parameter  $C_n^2$  were taken into consideration [7, 36-42]. The WT, MT and ST regimes are considered, for which we set  $C_n^2 = 4.74 \times 10^{-15} \text{m}^{-2/3}$ ,  $C_n^2 = 3.8 \times 10^{-14} \text{m}^{-2/3}$  and  $C_n^2 = 8.3 \times 10^{-14} \text{m}^{-2/3}$ , respectively, and  $l_{fso} = 1500 \text{ m}$  and  $2000 \text{ m}$  [7]. Using Eq. (1), the calculated Rytov variances are  $\sigma_R^2 = 0.2$  (WT),  $\sigma_R^2 = 1.60$  (MT),  $\sigma_R^2 = 3.51$  (ST), and  $\sigma_R^2 = 0.310$  (WT),  $\sigma_R^2 = 2.701$  (MT),  $\sigma_R^2 = 5.89$  (ST), for  $l_{fso} = 1500$  and  $2000 \text{ m}$ , respectively [7]. The DPPM thermal noise variance is back calculated using a bandwidth expansion factor such that  $\sigma_{th-DPPM}^2 = B_{exp} \sigma_{th-OOK}^2$  where  $B_{exp} = 2^M/M$  [7, 37, 42-46] is the DPPM bandwidth expansion factor and  $\sigma_{th-OOK}^2 = 7 \times 10^{-7} \text{ A}$  is obtained from a model of a positive-intrinsic-negative (PIN)-field effect transistor receiver with  $R_b = 2.5 \text{ Gbps}$  at BER of  $10^{-12}$  assuming a sensitivity of  $-23 \text{ dBm}$  [7, 38, 42-48]. The demux (or OBPF) channel bandwidth is  $80 \text{ GHz}$  with  $100 \text{ GHz}$  adjacent channel spacing, this is about the same with those seen in [39, 40] and will easily accommodate the slot rate of  $45.7 \text{ GHz}$  for maximum DPPM coding level of  $M = 7$  considered [7, 17, 46-50]. Typical values for adjacent channel rejection ratio ranges from  $-20 \text{ dB}$  to  $-30 \text{ dB}$  [7], [39-41], [50-54]. It can be deduced from the plots that the DPPM technique is capable of providing better performance when compared to the OOK-NRZ technique [7, 36-40, 48-54]. Fig. 3 shows BER vs. average power at receiver collecting lens (RCL) input (dBm) for DPPM and OOK using MCB, while  $M = 5$ ,  $l_{fso} = 2000 \text{ m}$ ,  $G = 30 \text{ dB}$ , and  $D_{RX} = 25 \text{ mm}$  for NT and (a) WT (b) MT (c) ST, (d) comparison for no turbulence and weak turbulence, that presented in [17], [Present], all with aperture averaging (AA). A comparison is made between DPPM at  $M = 5$  and an equivalent optically preamplified OOK-NRZ FSO system using  $l_{fso} = 1500 \text{ m}$ ,  $D_{RX} = 20 \text{ mm}$  and MCB method for both systems. At target BER (using MCB), DPPM offers about 10-11dB sensitivity improvements over the OOKNRZ-FSO system in the absence of turbulence [7, 42-47], [52-59]. When impaired by turbulence, the sensitivity improvement of DPPM over OOK-NRZ is reduced, respectively, to about 10 dB (WT), 8 dB (MT) and 8 dB, (ST) [Present]. An improvement of about 7 – 9 dB (depending on the turbulence level) can be potentially achieved using the DPPM scheme over an equivalent on off keyed non return-to-zero based FSO system that presented in [7, 17], [52]. When impaired by turbulence, the sensitivity improvement of DPPM over OOK-NRZ is reduced, respectively, to about 7 dB (WT), 8 dB (MT) and 8 dB, (ST) [7, 17], [46-49], [54-59].

**Table 1** Parameters used in calculations for Refs. [17, 42] and [Present Work Proposed]

Parameters	Description	Ref. [17]	Ref. [42]	Values [Present Work Proposed]
$R_b$	Binary data rate	2.5 Gbps	2.5 Gbps	2.5 Gbps
$B_{opt}$	Demux channel optical noise bandwidth	80 GHz	76 GHz	80 GHz
$\lambda_{sig}$	Signal wavelength	1550 nm	1550 nm	1550 nm
$\eta$	Receiver quantum efficiency	0.75	0.9	1
$G$	Optical preamplifier gain	30.6 dB or 8.8 dB	27 dB or 8 dB	30 dB
$NF$	Optical preamplifier noise figure	4.77 dB	4.77 dB	4.77 dB
$l_{fso}$	Optical link length	1000 m and 1500 m	1000 m and 1500 m	1500 m and 2000 m
$m_t$	Polarization states of ASE noise	2	2	2

Table 2 Design parameters required for a FSO link

Design Parameter	Symbol
Receiving lens diameter	$D_{RX}$
Beam divergence angle	$\varphi$
Optical link length	$l_{fso}$
Refractive index structure constant	$C_n^2$
Plane wave spatial coherence radius	$\rho_0$
Normalized pointing error standard deviation	$\sigma_{PE}/r_{RX}$

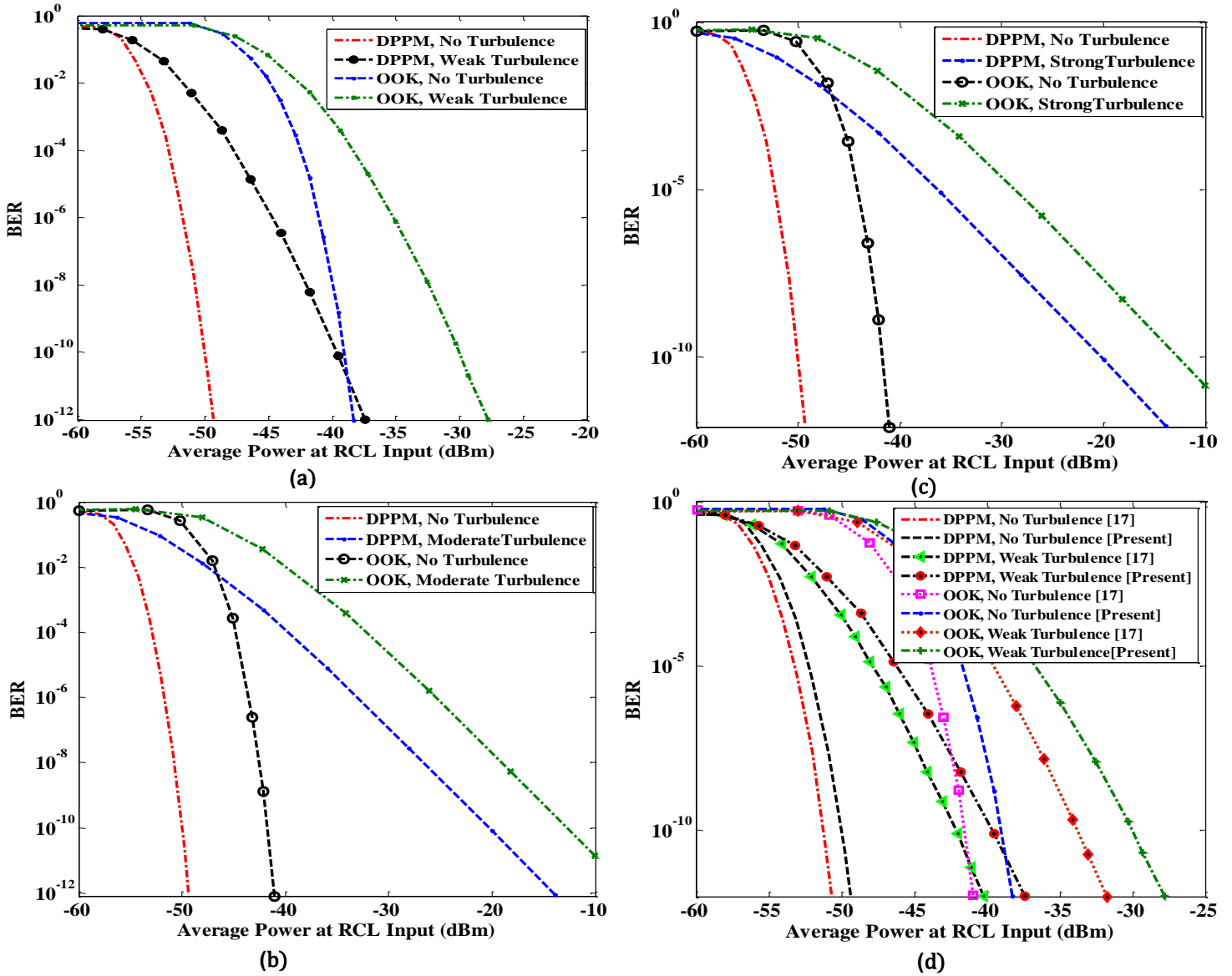


Fig. 3 BER vs. average power at receiver collecting lens (RCL) input (dBm) for DPPM and OOK using MCB, while  $M = 5$ ,  $l_{fso} = 2000$  m,  $G = 30$  dB, and  $D_{RX} = 25$  mm for NT. (a) WT, (b) MT, (c) ST, and (d) comparison for no turbulence and weak turbulence, that presented in [17], [present], all AA.

### 8. Conclusions

The study presented in this paper highlights the impact of combined turbulence and pointing error on an optically preamplified DPPM FSO communication system. The research delves into modeling the Bit Error Rate for

an optically preamplified OOK FSO system operating under atmospheric turbulence using MGF-based methods like CB and MCB. The DPPM scheme emerges as a promising avenue for enhancing FSO power efficiency further, showcasing considerable enhancements over OOK NRZ across various conditions. The findings indicate a notable enhancement in receiver sensitivity when utilizing the DPPM technique compared to OOK NRZ. Additionally, the utilization of aperture-averaging as a turbulence mitigation strategy is demonstrated, with results showcasing marked improvements, particularly in the MT and ST regimes.

**Ethical Approval:** Not applicable

**Conflict of Interest:** The authors declare no conflicts of interest.

**Authors' contributions:** **Ebrahim Eldesoky Elsayed:** Conceptualization, Formal analysis, Resources, Data curation, Planning, Execution, Writing-review & Editing, Visualization, Software, Implementation, Programming, Writing-original draft, Investigations, Validations, and Project administration. **Mohammed Raisan Hayal:** Visualization, Formal analysis, Resources, Data curation, Investigations, Methodology, Proofreading, Software, Planning, Execution, Writing & Editing, Review, and Validations.

**Funding:** This study did not receive any external funding.

**Availability of data and materials:** Data is provided under the request.

**Acknowledgment:** We sincerely thank the editor and reviewers for their diligent efforts in enhancing our manuscript.

## References

1. Andrews, L.C., Phillips, R.L. (2005). 'Laser beam propagation through random media' (SPIE Press, Bellingham, Washington, 2nd edn)
2. Caplan, D.O. (2007). 'Laser communication transmitter and receiver design', *J. Opt. Fibre Commun. Rep.*, 4, pp. 225–362
3. Majumdar, A.K. (2005). 'Free-space laser communication performance in the atmospheric channel', *J. Opt. Fiber Commun. Res.*, 2, pp. 345–396
4. Mukherjee, B. (2000). 'WDM optical communication networks: progress and challenges', *IEEE J. Sel. Areas Commun.*, 2000, 18, (10), pp. 1810–1824
5. Ciaramella, E., Arimoto, Y., Contestabile, G., et al. (2009). '1.28 Terabit/s ( $32 \times 40$  Gbit/s) wdm transmission system for free space optical communications', *IEEE J. Sel. Areas Commun.*, 27, (9), pp. 1639–1645
6. Forin, D.M., Beleffi, G.M.T., Curti, F., et al. (2007). 'On field test of a wavelength division multiplexing free space optics transmission at very high bit rates'. Ninth Int. Conf. Telecommunication, pp. 77–80
7. Ebrahim E. Elsayed and Bedir B. Yousif, "Performance enhancement of M-ary pulse-position modulation for a wavelength division multiplexing free-space optical systems impaired by interchannel crosstalk, pointing error, and ASE noise", *Optics Communications*, vol. 475, pp. 126219, (15 November 2020).
8. Zuo, T.J., Phillips, A.J. (2009). 'Performance of burst-mode receivers for optical digital pulse position modulation in passive optical network application', *IET Optoelectron.*, 3, (3), pp. 123–130, 2009
9. Bongtae, K., Byoung-Whi, K.: 'WDM-PON development and deployment as a present optical access solution'. Conf. on Optical Fiber Communications – includes Post Deadline Papers, pp. 1–3
10. Nirmalathas, Ke, Lim, W., Skafidas, A., C., E. (2011) '4 × 12.5 Gb/s WDM optical wireless communication system for indoor applications', *J. Lightwave Technol.*, 29, (13), pp. 1988–1996, 2011
11. Aladeloba, A.O., Woolfson, M.S., Phillips, A.J. (2013) 'WDM FSO network with turbulence-accentuated interchannel crosstalk', *J. Opt. Commun. Netw.*, 5, (6), pp. 641–651
12. Gee-Kung, C., Chowdhury, A., Zhensheng, J., et al. (2009). 'Key technologies of WDM-PON for future converged optical broadband access networks [invited]', *IEEE/OSA J. Opt. Commun. Netw.*, 1, (4), pp. C35–C50
13. Kazovsky, L., Shing-Wa, W., Ayhan, T., Albeyoglu, K.M., Ribeiro, M.R.N., Shastri, A. (2012). 'Hybrid optical-wireless access networks', *Proc. IEEE*, 100, (5), pp. 1197–1225
14. Liaw, S.K., Lai, Y.T., Chang, C.L., Shung, O. (2008). 'AWG-based WDM-PON monitoring system using an optical switch and a WDM filter', *Laser Phys.*, 18, (9), pp. 1052–1055
15. Phillips, A.J., Cryan, R.A., Senior, J.M. (1996). 'An optically preamplified intersatellite PPM receiver employing maximum likelihood detection', *IEEE Photon. Technol. Lett.*, 8, (5), pp. 691–693
16. Muhammad, S.S., Gappmair, W., Leitgeb, E. (2006). 'PPM channel capacity evaluation for terrestrial FSO links'. Proc. Int. Workshop on Satellite and Space Communication, pp. 222–226

17. Aladeloba, A.O., Phillips, A.J., Woolfson, M.S. (2012). 'Performance evaluation of optically preamplified digital pulse position modulation turbulent free-space optical communication systems', *IET Optoelectron.*, 6, (1), pp. 66–74
18. Aldibbiat, N.M., Ghassemlooy, Z., McLaughlin, R. (2005) 'Indoor optical wireless systems employing dual header pulse interval modulation (DH-PIM)', *Int. J. Commun. Syst.*, 18, (3), pp. 285–305
19. Ghassemlooy, Z., Popoola, W., Rajbhandari, S.: 'Optical wireless communications – system and channel modelling with MATLAB' (CRC Press, London, 1st edn, 2013)
20. Farid, A. A., Hranilovic, S. (2007) Outage capacity optimization for free-space optical links with pointing errors, *J. Lightwave Technol.*, vol. 25, no. 7, pp. 1702-1710
21. Sandalidis, H. G., et al.: BER performance of FSO links over strong atmospheric turbulence channels with pointing errors, *IEEE Communications Letters*, vol. 12, no. 1, pp. 44-46, 2008
22. Aladeloba, A. O., et al.: Improved bit error rate evaluation for optically pre-amplified free-space optical communication systems in turbulent atmosphere, *IET Optoelectronics*, vol. 6, pp. 26-33, Feb. 2012
23. Yamamoto, Y., "Noise and error rate performance of semiconductor laser amplifiers in PCM-IM optical transmission systems," *IEEE Journal of Quantum Electronics*, vol. 16, no. 10, pp. 1073-1081, Oct. 1980
24. Personick, S. D., "Applications for quantum amplifiers in simple digital optical communication systems," *Bell System Technical Journal*, vol. 52, no. 1, pp. 117-133, Jan. 1973
25. Ribeiro, L. F. B., Da Rocha, J. R. F., and Pinto, J. L., "Performance evaluation of EDFA preamplified receivers taking into account intersymbol interference," *Journal of Lightwave Technology*, vol. 13, no. 2, pp. 225-232, Feb. 1995
26. Abtahi, M., Lemieux, P., Mathlouthi, W., Rusch, L.A.: 'Suppression of turbulence-induced scintillation in free-space optical communication systems using saturated optical amplifiers', *J. Lightwave Technol.*, 24, (12), pp. 4966–4973, 2006
27. Lesson, M. S., "Pulse position modulation for spectrum-sliced transmission," *IEEE Photonic Technology Letter*, vol. 4, no. 3, pp. 1191-1193, Apr. 2004
28. Davidson, F. M. and Sun, X. M., "Slot clock recovery in optical PPM communication systems with Avalanche photodiode photodetectors," *IEEE Trans. Commun.*, vol. 37, no. 11, pp. 1164- 1172, Nov. 1989
29. Sun, X. M. and Davidson, F. M., "Word timing recovery in direct detection optical PPM communication systems with Avalanche photodiodes using a phase lock loop," *IEEE Trans. Commun.*, vol. 38, no. 5, pp. 666-673, May 1990
30. Karp, S., Gagliardi, R.M., Moran, S.E., Stotts, L.B.: 'Optical channels: fibers clouds water and the atmosphere' (Plenum Press, New York,1988)
31. Zhu, X., Kahn, J.M.: 'Free-space optical communication through atmospheric turbulence channels', *IEEE Trans. Commun.*, 50, (8), pp. 1293–1300, 2002
32. Al-Habash, M.A., Andrews, L.C., Phillips, R.L.: 'Mathematical model for the irradiance probability density function of a laser beam propagating through turbulent media', *Opt. Eng.*, 40, (8), pp. 1554–1562, 2001
33. Khalighi, M.A., Schwartz, N., Aitamer, N., Bourennane, S.: 'Fading reduction by aperture averaging and spatial diversity in optical wireless systems', *IEEE/OSA J. Opt. Commun. Netw.*, 1, (6), pp. 580–593, 2009
34. Vetelino, F.S., Young, C., Andrews, L.: 'Fade statistics and aperture averaging for Gaussian beam waves in moderate-to-strong turbulence', *Appl. Opt.*, 46, (18), pp. 3780–3789, 2007
35. Yuksel, H., Davis, C.: 'Aperture averaging experiment for optimizing receiver design and analyzing turbulence on free-space optical communication links'. *Conf. on Lasers and Electro-Optics (CLEO)*, Baltimore, MD, USA, pp. 743–745, May 2005
36. Aladeloba, A. O., Phillips, A. J., and Woolfson, M. S., "DPPM FSO communication systems impaired by turbulence, pointing error and ASE noise," in *14th Int. Conf. on Transparent Optical Networks (ICTON)*, Coventry, UK, 2012
37. Sibley, M.J.: 'Optical communications' (Macmillian Press Ltd, London, 2nd edn, 1995.)
38. Ramaswami, R., Sivarajan, K. N., Sasaki, G. H. *Optical Networks: A Practical Perspective*. 3rd ed. Boston: Morgan Kaufmann Publishers; 2010
39. Mizumoto, Maru, K., Uetsuka, T., , H.: 'Demonstration of Flat-Passband Multi/Demultiplexer Using Multi-Input Arrayed Waveguide Grating Combined With Cascaded Mach-Zehnder Interferometers'. *J. Lightw. Technol.*, 25, (8), pp.2187-2197, 2007
40. Hirano, A., Miyamoto, Y., Kuwahara, S.: 'Performances of CSRZ-DPSK and RZDPSK in 43-Gbit/s/ch DWDM G.652 single-mode-fiber transmission'. *Optical Fiber Commun. Conf.*, 2003, pp. 454-456, 2003
41. Yu, C. X., Neilson, D. T.: 'Diffraction-grating-based (de)multiplexer using image plane transformations'. *IEEE J. Selected Topics in Quantum Electronics*, 2002, 8, (6), pp. 1194-1201, 2002
42. Mbah, A.M., Walker, J.G., Phillips, A.J.: 'Performance evaluation of digital pulse position modulation for wavelength division multiplexing FSO systems impaired by interchannel crosstalk', *IET Optoelectron.*, 8, (6), pp. 245–255, 2014
43. Henry, P. S., Error-rate performance of optical amplifiers, *Optical Fiber Communication Conference*, Houston, Texas, vol. 5, Feb. 1989

44. ZhaoZ, Z., Tan, J., Liu, Y., Liu, J.: '200 Gb/s FSO WDM Communication System Empowered by Multiwavelength Directly Modulated TOSA for 5G Wireless Networks', *IEEE Photonics Journal*, vol. 10, no. 4, pp. 1943-0655, Aug. 2018
45. eprints.nottingham.ac.uk, 2018
46. Hien T. T. Pham., Ngoc T. Dang: Performance improvement of spatial modulation-assisted FSO systems over Gamma-Gamma fading channels with geometric spreading, *Photon Netw Commun*, 34, pp.213-220, 2017
47. E. E. Elsayed and B. B. Yousif, "Performance evaluation and enhancement of the modified OOK based IM/DD techniques for hybrid fiber/FSO communication over WDM-PON systems," *Opt. Quantum Electron.*, vol. 52, no. 9, 2020, doi: 10.1007/s11082-020-02497-0.
48. B. B. Yousif, E. E. Elsayed, and M. M. Alzalabani, "Atmospheric turbulence mitigation using spatial mode multiplexing and modified pulse position modulation in hybrid RF/FSO orbital-angular-momentum multiplexed based on MIMO wireless communications system," *Opt. Commun.*, vol. 436, pp. 197-208, 2019, doi: 10.1016/j.optcom.2018.12.034.
49. A. M. Mbah, J. G. Walker, and A. J. Phillips, "Outage probability of WDM free-space optical systems affected by turbulence-accentuated interchannel crosstalk," *IET Optoelectron.*, vol. 11, no. 3, pp. 91-97, 2017, doi: 10.1049/iet-opt.2016.0057.
50. B. B. Yousif and E. E. Elsayed, "Performance Enhancement of an Orbital-Angular-Momentum-Multiplexed Free-Space Optical Link under Atmospheric Turbulence Effects Using Spatial-Mode Multiplexing and Hybrid Diversity Based on Adaptive MIMO Equalization," *IEEE Access*, vol. 7, pp. 84401-84412, 2019, doi: 10.1109/ACCESS.2019.2924531.
51. E. E. Elsayed and B. B. Yousif, "Performance enhancement of hybrid diversity for M-ary modified pulse-position modulation and spatial modulation of MIMO-FSO systems under the atmospheric turbulence effects with geometric spreading," *Opt. Quantum Electron.*, vol. 52, no. 12, 2020, doi: 10.1007/s11082-020-02612-1.
52. Elsayed, E. E., & Yousif, B. B. (2020). Performance enhancement of M-ary pulse-position modulation for a wavelength division multiplexing free-space optical systems impaired by interchannel crosstalk, pointing error, and ASE noise. *Optics Communications*, 475. <https://doi.org/10.1016/j.optcom.2020.126219>
53. Ebrahim E. Elsayed, Bedir B. Yousif, and Mahmoud M. Alzalabani, "Performance enhancement of the power penalty in DWDM FSO communication using DPPM and OOK modulation", *Optical and Quantum Electronics*, vol. 50 (7), pp. 282, (26 June 2018).
54. Ansari, N., Zhang, J.: 'Media access control and resource allocation for next generation passive optical networks' (Springer, 2013)
55. Ebrahim E. Elsayed and Bedir B. Yousif, "Performance enhancement of the average spectral efficiency using an aperture averaging and spatial-coherence diversity based on the modified-PPM modulation for MISO FSO links", *Optics Communications*, vol. 463, pp. 125463, (15 May 2020).
56. Elsayed, E.E., Yousif, B.B. Performance enhancement of hybrid diversity for M-ary modified pulse-position modulation and spatial modulation of MIMO-FSO systems under the atmospheric turbulence effects with geometric spreading. *Opt Quant Electron* 52, 508 (2020). <https://doi.org/10.1007/s11082-020-02612-1>
57. Elsayed, E.E., Yousif, B.B. & Singh, M. Performance enhancement of hybrid fiber wavelength division multiplexing passive optical network FSO systems using M-ary DPPM techniques under interchannel crosstalk and atmospheric turbulence. *Opt Quant Electron* 54, 116 (2022). <https://doi.org/10.1007/s11082-021-03485-8>
58. Elsayed, E. E., Alharbi, A. G., Singh, M., & Grover, A. (2022). Investigations on wavelength-division multiplexed fibre/FSO PON system employing DPPM scheme. *Optical and Quantum Electronics*, 54(6). <https://doi.org/10.1007/s11082-022-03717-5>
59. Elsayed, E.E., Kakati, D., Singh, M. et al. Design and analysis of a dense wavelength-division multiplexed integrated PON-FSO system using modified OOK/DPPM modulation schemes over atmospheric turbulences. *Opt Quant Electron* 54, 768 (2022). <https://doi.org/10.1007/s11082-022-04142-4>

